Effects of dispersion corrections on the theoretical description of bulk metals

Adebayo A. Adeleke and Erin R. Johnson*
Department of Chemistry, Dalhousie University, 6274 Coburg Road, Halifax, NS, Canada B3H 4R2

(Received 29 October 2022; revised 23 December 2022; accepted 19 January 2023; published 3 February 2023)

The addition of a London dispersion correction to standard Kohn-Sham density-functional theory is essential for an accurate description of noncovalent interactions. While several dispersion-corrected density functionals (DC-DFs) have shown excellent performance for hard solids at ambient conditions, their transferability to metallic systems at ambient conditions or under isotropic compression has not been systematically examined. In this study, we assess the ability of selected DC-DFs to describe the equations of state (EOSs) of selected elemental metals and intermetallic compounds up to several gigapascals of pressure. EOS-derived properties, such as the unit-cell volume, the bulk modulus, and its pressure derivative, were then evaluated with and without thermal effects and the results compared with experimental reference data. We also assess the ability of the DC-DFs to predict the phase-transition pressures for a set of intermetallic compounds. The results of this study establish that London dispersion physics, and even dispersion contributions from the core electrons, is important in the description of bulk metals.

DOI: 10.1103/PhysRevB.107.064101

I. INTRODUCTION

The equation of state (EOS) is a thermodynamic relation from which many fundamental properties of condensed phases of materials can be derived. The EOS is key to the understanding of planetary interiors, as well as dynamical study of high-energy processes and high-energy density materials [1,2]. Advancement in experimental methods and the reduction of systematic uncertainty have led to improved accuracy in the accretion of hydrostatic compression data on metals up to a few hundreds of gigapascal (GPa) [3,4]. However, miniaturization of the sample increases as higher pressures are approached, leaving many extreme-pressure regions of the EOS unexplored and leading to the continual need for accurate theoretical predictions. Thus, concerted efforts are being made to improve the agreement between experimental and theoretical EOSs through the development of improved electronic-structure methods [5], particularly within the framework of density-functional theory (DFT) [6,7].

Over the years, the field of DFT has witnessed the development of a hierarchy of density functionals (DFs), including generalized gradient approximations (GGAs) [8–12], meta-GGAs [13–18], and hybrids [19–22]. DFs are widely employed for materials simulations, involving the prediction of structure and lattice energies, among other properties [23–25]. However, due to approximations involved in the development of these DFs, they generally provide an incomplete representation of exchange-correlation interactions between electrons. This drawback suggests that some important energy terms may be missing, and accounting for them should improve the performance of DFT predictions. One such term has been identified as the London dispersion force [26–30], which is a long-range, highly nonlocal form of electron correlation.

London dispersion, the weakest van der Waals force, originates from instantaneous charge oscillations that induce the formation of dipoles and higher-order multipoles. Dispersion forces can influence phase changes [31,32], packing in molecular crystals [33–35], and surface adsorption [36,37]. While they are routinely applied to all types of solids, standard DFs do not capture London dispersion. Thus, inclusion of dispersion physics within DF approximations is very important for an accurate determination of the structural and energetic properties of molecular systems [38,39], crystals [40,41], and layered materials [42–44]. Inclusion of dispersion has also been shown to improve the predicted properties of hard solids [45,46], such as lattice parameters, bulk moduli, and lattice energies. Unlike molecular and ionic solids, the importance of dispersion has not yet been well established for metals. This is likely because these three classes of materials are characterized by different bonding types—namely metallic bonds, electrostatics, and van der Waals interactions (including hydrogen and halogen bonding), respectively.

Dispersion energies (E_{disp}) are commonly computed as a correction term to the base DF energy (E_{base}), such that the total energy becomes

$$E_{\text{DFT}} = E_{\text{base}} + E_{\text{disp}}. \tag{1}$$

Several dispersion correction models based on second-order perturbation theory have been proposed, such as the Tkatchenko-Scheffler (TS) [47], Grimme's DFT-D2 [48], DFT-D3 [49,50], DFT-D4 [51,52], and the exchange-hole dipole moment (XDM) [53,54] methods. These are colloquially referred to as asymptotic dispersion corrections. Other models in this category include the many-body dispersion (MBD) method [55,56] and its modified forms—MBD-FI [57] and uMBD [58]. Beyond evaluation of a separate E_{disp} term, certain DFs contain a dispersion correction built into the exchange-correlation functional, which is evaluated along with the base energy during each self-consistent-field (SCF)

*erin.johnson@dal.ca

cycle. These include the van der Waals DFs [59–61] and the Vydrov–Van Voorhis [62,63] series.

Despite the widespread success of dispersion corrections across molecular and solid-state systems, their application beyond ambient conditions remains scarce [64–66], particularly for solids [43,67,68]. Perhaps systems under high compression are thought to be closely packed to the point where dispersion forces are negligible—a conjecture that has yet to be substantiated or disproved. While computational studies of bulk metals (using standard, non-dispersion-corrected DFs) up to several hundreds of GPa are ubiquitous in the literature [3,4,69–72], none has systematically examined the performance of dispersion models in accurately describing the EOS of bulk metals. Against this backdrop, it is important to understand the effects of dispersion on the predicted properties of homoatomic and heteroatomic metals. One way to achieve this is through a benchmark study.

This work examines the influence of dispersion on the EOS and EOS-derived properties—the unit-cell volume, the bulk modulus, its pressure derivative, and the phase-transition pressure—for an ensemble of elemental metals and intermetallic compounds. The results demonstrate the effects of dispersion and core states on the theoretical prediction of the EOS and EOS-derived properties of bulk metals. Overall, we find that pairing selected DFs with the exchange-hole dipole moment (XDM) or Grimme's D3 dispersion methods generally leads to better agreement with experimental reference data. Our results also reiterate the importance of thermal corrections in improving agreement between experimental and theoretical EOS.

II. COMPUTATIONAL METHODS

In this work, calculations were performed with and without inclusion of thermal expansion to demonstrate the interplay between dispersion and thermal corrections. We limit ourselves to GGA functionals due to the significantly higher mathematical complexity and nonavailability of geometry relaxation with meta-GGAs in open-source plane-wave DFT codes. We further consider only post-SCF dispersion corrections of the type given by Eq. (1). To rule out a dependence on implementation, two sets of simulations were performed using (i) plane-wave DFT with the projector augmented-wave (PAW) method [73], and (ii) all-electron calculations with numeric atom-centered orbitals (NAOs) [74].

PAW calculations were performed using QUANTUM ESPRESSO (QE) version 6.7 [75], while the NAO calculations used the Fritz Haber Institute *ab initio* materials simulations (FHI-aims) package [74]. The GGA functionals considered are PBEsol [12], PBE [8], and B86bPBE [8,9]. PBEsol was not paired with any dispersion correction since it is accepted to perform very well for predicting the ambient properties of bulk solids [76]. PBE was paired with a selection of dispersion corrections—TS [47] (FHI-aims), Grimme's D3 method with [49] and without [50] Becke-Johnson (BJ) damping [77] (QE), and XDM [53,54,78] (both QE and FHI-aims). Finally, XDM was also paired with the B86bPBE functional (again using both QE and FHI-aims), as this combination has proven optimal for molecular dimers and crystals [30,40,78]. Computational settings, including cutoffs and **k**-point meshes, for all the systems considered in this study are given in the Supplemental Material [79] and Refs. [78,80].

We prepared a benchmark set of elemental metals made up of both nonmagnetic and magnetic materials: Al, FM-α-Fe, FM-Ni, Cu, Zn, Mo Ag, Ta, W, Pt, and Au [3,4]. Here, FM denotes a ferromagnetic configuration. We also prepared another set of intermetallic compounds: FM-Fe_3Sn, FM-Fe_3Sn_2 [81], α-$AuAl_2$ [82], α-$SrAl_2$, β-$SrAl_2$ [83–85], $PtIn_2$ [86], and $AuIn_2$ [87]. A third benchmark set was prepared comprised of a collection of intermetallic compounds with experimentally known phase-transition pressures: Na_3Bi, $ScGa_2$, LiCd [88], $AuAl_2$ [82], and $SrAl_2$ [83–85]. These sets will be referred to as the EM11, IM07, and PT05 sets for the elemental metals, intermetallic compounds, and phase transitions, respectively. All the metals in the EM11 benchmark set have a cubic crystal lattice system (either body-centered-cubic or face-centered-cubic structures), except for Zn, which has a hexagonal-close-packed structure. For the IM07 benchmark, four of the intermetallic compounds have face-centered-cubic structures, while Fe_3Sn is orthorhombic, $PtIn_2$ is hexagonal, and $AuIn_2$ is tetragonal.

For all systems in this study, our experimental reference corresponds to room-temperature compression data. There are two computationally different, but theoretically equivalent, methods of obtaining compression data: geometry optimization to obtain pressure-volume data or fitting some energy-volume points to an empirical EOS [89]. We have employed both methods in this study, albeit for different analyses. Computationally, we introduce isotropic pressure to the elemental metals and intermetallic compounds adiabatically. For each metal, the pressure range was chosen to bracket the pressure covered by the experimental reference data. All of the metals considered are stable under applied pressure and do not undergo any spontaneous phase transition during geometry optimization, nor do they undergo any electronic (metal to semiconductor) transitions, within the pressure range reported.

Computed pressure-volume data for the EM11 and IM07 sets were fitted using either the Vinet [90] or the third-order Birch-Murnaghan [91–93] forms for the EOS, respectively. The different choice of EOS fitting model between the two benchmark sets is driven by the desire for direct comparison with the reference data. In the Vinet EOS, the pressure, P, is given by

$$P = 3B_0\left(\frac{V}{V_0}\right)^{-\frac{2}{3}}\left[1-\left(\frac{V}{V_0}\right)^{\frac{1}{3}}\right] \times \exp\left\{\frac{3}{2}(B_0'-1)\left[1-\left(\frac{V}{V_0}\right)^{\frac{1}{3}}\right]\right\}, \quad (2)$$

where V is the unit-cell volume. Conversely, the third-order Birch-Murnaghan formulation of the EOS is expressed as

$$P = \frac{3}{2}B_0\left[\left(\frac{V_0}{V}\right)^{\frac{7}{3}}-\left(\frac{V_0}{V}\right)^{\frac{5}{3}}\right] \times \left[1+\frac{3}{4}(B_0'-4)\left\{\left(\frac{V_0}{V}\right)^{\frac{2}{3}}-1\right\}\right]. \quad (3)$$

In both EOSs, the three fitted parameters are the unit-cell volume, V_0, the isothermal bulk modulus,

$$B_0 = -V\left.\frac{\partial P}{\partial V}\right|_{V=V_0} = \left(V\frac{\partial^2 E}{\partial V^2}\right)\Big|_{V=V_0}, \tag{4}$$

and its pressure derivative,

$$B_0' = \left.\frac{\partial B_0}{\partial P}\right|_{V=V_0}, \tag{5}$$

all at ambient pressure. This analysis yields data for cold compression, without inclusion of thermal effects.

For room-temperature compression, the pressure-volume data were switched to energy-volume data, and the corresponding transformations of the Vinet [94,95] and Birch-Murnaghan [92] EOSs were used. The temperature-dependent properties were computed using Gibbs free energies,

$$G(V,T) = E(V) + F_{\text{vib}}(V,T), \tag{6}$$

where $E(V)$ is the static DFT electronic energy at a given volume and zero temperature, and F_{vib} is the vibrational free energy at a finite temperature. The $G(V,T)$ data spanning the compression volumes are then fitted to the appropriate EOS model [92,94,95] for the computation of V_{th}, B_{th}, and B'_{th}. In addition to these properties, the total pressure experienced by the system becomes the sum of the static (0 K) and the thermal (293 K) pressures, which is expressed as

$$P_{\text{total}} = -\frac{\partial G(V,T)}{\partial V_{\text{th}}}. \tag{7}$$

The phase-transition pressure in the PT05 benchmark set was assessed using the computed P_{total}.

Finally, we estimated the F_{vib} contribution using the empirical Debye model [96] according to

$$F_{\text{vib}}(V,T) = \frac{9}{8}k_{\text{B}}\Theta_{\text{D}} + k_{\text{B}}T\left\{3\ln\left[1-\exp\left(-\frac{\Theta_{\text{D}}}{T}\right)\right] - D\left(\frac{\Theta_{\text{D}}}{T}\right)\right\}, \tag{8}$$

where $D(\frac{\Theta_{\text{D}}}{T})$ is the Debye function defined as

$$D(\chi) = \frac{3}{\chi^3}\int_0^{\chi}\frac{t^3}{e^t-1}dt. \tag{9}$$

The Debye temperature, Θ_{D}, is obtained via the Debye-Wang model [97] according to

$$\Theta_{\text{D}} = \alpha\frac{(6\pi^2)^{\frac{1}{3}}\hbar}{k_B}V^{\frac{1}{6}}\left\{\frac{1}{M}\left[B - \frac{2(\lambda+1)}{3}P\right]\right\}^{\frac{1}{2}}. \tag{10}$$

In this equation, $P = -\frac{dE}{dV}$, $B = (V\frac{\partial^2 E}{\partial V^2})$, M is the atomic mass per unit cell, $\hbar$ is the reduced Planck constant, and k_B is Boltzmann's constant. Since the thermal contribution is evaluated at a room temperature of $T = 293$ K, the adjustable Debye-Wang parameter is set to $\lambda = 1$. For the nonmagnetic metals in our sets, we chose a scaling factor of $\alpha = 0.617$ [98], while $\alpha = 0.764$ [99] was used for the magnetic systems.

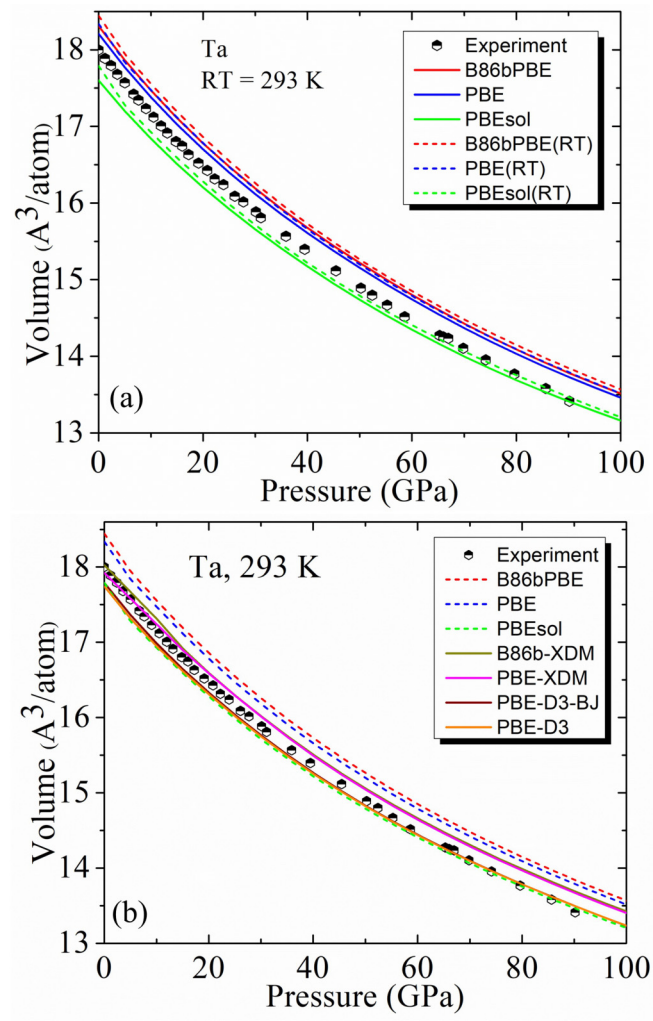

FIG. 1. Illustration of the effects of temperature correction (top) and dispersion correction (bottom) on the computed EOS of tantalum (Ta). The theoretical EOSs were calculated using the PAW method and are compared with experimental compression data from Refs. [3,4].

III. RESULTS

A. Effects of thermal expansion on the EOS

Changing temperature alters the volume of a material and has a direct effect on other physical properties. Thus, applying temperature correction to static DF calculations can improve the agreement between theoretical prediction of volume and bulk modulus (or incompressibility) and the corresponding experimentally measured values. The effect of thermal correction on the EOS of metals is exemplified using tantalum (Ta) in a body-centered-cubic cell (Fig. 1), which is a member of our EM11 benchmark set. As shown in Fig. 1(a), accounting for temperature effects generally leads to volume expansion, since increasing the temperature increases the kinetic energy through the lattice vibrations. The resulting effect is a slight (harmonic) or large (anharmonic) increase in the distance between neighboring atoms or molecules, proportional to the temperature, which leads to an expanded unit cell. Inclusion of thermal expansion also results in lowering of the bulk modulus

TABLE I. Mean errors (MEs) and mean absolute errors (MAEs) in unit-cell volumes, in Å^3, computed with selected density functionals and dispersion corrections. The results correspond to the thermally corrected volumes (V_{th}) in the absence of applied pressure, while the static volumes (V_0) are given in parentheses. Errors are shown for the EM11 and IM07 benchmarks separately, as well as for the combined data set.

		EM11				IM07				Combined			
	Method	ME		MAE		ME		MAE		ME		MAE	
QE	PBEsol	−0.11	(−0.38)	0.31	(0.44)	0.17	(−0.22)	1.20	(1.08)	0.00	(−0.31)	0.65	(0.69)
	PBE	0.60	(0.32)	0.65	(0.41)	1.08	(0.66)	1.66	(1.36)	0.79	(0.45)	1.04	(0.78)
	B86bPBE	0.74	(0.45)	0.77	(0.51)	1.27	(0.81)	1.80	(1.47)	0.95	(0.59)	1.17	(0.88)
	PBE-D3	0.02	(−0.23)	0.26	(0.34)	0.33	(0.06)	1.34	(1.22)	0.14	(−0.17)	0.68	(0.68)
	PBE-D3BJ	0.00	(−0.30)	0.28	(0.42)	0.23	(−0.15)	1.29	(1.16)	0.09	(−0.24)	0.67	(0.71)
	PBE-XDM	0.40	(0.08)	0.50	(0.42)	−0.35	(−0.79)	1.00	(1.04)	0.11	(−0.26)	0.70	(0.66)
	B86bPBE-XDM	0.38	(0.04)	0.54	(0.49)	0.03	(−0.49)	1.26	(1.14)	0.24	(−0.16)	0.82	(0.74)
FHI-aims	PBEsol	−0.15	(−0.44)	0.31	(0.45)	0.31	(−0.03)	1.17	(1.09)	0.03	(−0.28)	0.64	(0.70)
	PBE	0.54	(0.22)	0.59	(0.42)	1.39	(0.84)	1.39	(1.40)	0.87	(0.46)	0.90	(0.80)
	B86bPBE	0.67	(0.35)	0.67	(0.47)	1.44	(1.02)	1.75	(1.48)	0.97	(0.61)	1.09	(0.86)
	PBE-TS	−0.36	(−0.62)	0.68	(0.73)	−0.43	(−0.78)	1.34	(1.33)	−0.39	(−0.68)	0.94	(0.96)
	PBE-XDM	0.10	(−0.27)	0.41	(0.47)	−0.03	(−0.51)	1.05	(1.05)	0.05	(−0.36)	0.66	(0.69)
	B86bPBE-XDM	−0.01	(−0.31)	0.43	(0.50)	0.08	(−0.42)	1.14	(1.04)	0.03	(−0.36)	0.70	(0.71)

through relaxing the curvature of $E(V)$, which translates to a softening of the $P(V)$ relation. As $V(P)$ plots are shown in Fig. 1(a), the lower bulk modulus can be seen as a higher slope at $P = 0$.

Some DFT studies directly compare computed static properties with experimental data, which assumes that the thermal corrections are negligible, or relies on error cancellation between the DF and the thermal correction. Figure 1(a) shows that thermal correction improves agreement with the experimental EOS for PBEsol, but it leads to larger errors for the other GGAs. From Fig. 1(b), pairing GGAs with various dispersion models has the opposite effect to thermal correction, resulting in more compressed cell volumes and increased bulk modulus through increasing the curvature of $E(V)$, reflected in a more gradual slope at $P = 0$. It is the opposing signs of the thermal and dispersion corrections to physical properties, such as the volume and bulk modulus, that has led to the omission of both in many DFT studies of materials.

For the Ta example, we note that the XDM-corrected functionals provide the best agreement with the experimental EOS at low pressures, while PBEsol, PBE-D3, and PBE-D3(BJ) perform best at high pressures. The EOSs of the other metals considered are collected in the Supplemental Material [79]. Generally, there is a larger spread in the computed volumes at low pressure than at high pressure between the various (DC-)DFs, and no one method can provide consistently good EOS predictions for all metals. For Ag, Pt, and Au, all the computed curves are shifted to larger volumes than the experimental EOS, while the computed curves for Al, Cu, and W also reflect larger volumes than the experimental EOS, but only at very high pressures. This suggests that we are potentially underestimating the effects of dispersion and/or overestimating the effects of thermal expansion.

B. Equilibrium volumes

Table I shows the error statistics for the computed unit-cell volumes obtained for the EM11 and IM07 benchmarks using selected (DC-)DF methods. Results are given for calculations performed with, and without, thermal corrections. As expected based on the discussion of thermal expansion above, the mean errors (MEs) are uniformly shifted toward more positive values for the thermally corrected, compared to static, volumes. Notably, the mean absolute errors (MAEs) are roughly two to three times higher for the IM07 set, relative to the EM11, across all methods considered. This suggests that errors in the cell volumes may be constituent additive, perhaps due to the introduction of some errors from charge transfer [45,100] between the elemental metals that form the intermetallic compounds.

The volume errors observed for bcc-Fe (on the order of 1 Å^3) are very much larger than those obtained for the other metals in the EM11 set. Significantly better agreement with the experimental reference data can be achieved by adding a Hubbard U correction [101] to Fe, and we performed additional GGA+U calculations using QUANTUM ESPRESSO for all species containing Fe and Ni, with their Coulomb interaction potential (U) values set to 2.5 and 2.4 eV, respectively [102]. While the U values should properly change with pressure, using a constant U has been shown to have a minimal effect on EOS-derived properties [103]. The GGA+U results are shown in the Supplemental Material [79]; overall, this correction expands the cell volume, but also increases the magnetization from ∼2 to 3μ_B/atom. However, since geometry optimizations with GGA+U are not currently possible with FHI-aims, this correction is not included in the remainder of this work to allow for a direct comparison between the pseudopotential and all-electron results.

Without a dispersion correction, the MEs in Table I follow a general trend of PBEsol ≪ PBE < B86bPBE for both benchmark sets and with both electronic-structure codes. This trend follows the known exchange enhancement behavior of these functionals [30,104–107]. In the limit of large reduced density gradients, B86bPBE has the highest enhancement factor, and the best agreement with exact exchange, while PBE and PBEsol have similar enhancement factors [30]. However, this regime is not sampled by the density distributions in bulk metals, so we focus on behavior for small to moderate

gradients. Here, PBEsol has an enhancement factor that is significantly lower than either B86b or PBE, which leads to increased binding and smaller lattice constants. The PBEsol static volumes tend to underestimate the experimental cell volumes, while the static volumes from PBE and B86bPBE are systematically too large. Inclusion of thermal expansion therefore improves agreement between the PBEsol V_{th} values and experiment, while further worsening agreement for PBE and B86bPBE. Consistent with literature findings, PBEsol with thermal correction performs quite well for prediction of unit-cell volumes of simple metals [108].

The good performance of PBEsol, without any dispersion correction, is not surprising as it was designed specifically for solids. PBEsol does not account for the long-range electron correlation responsible for dispersion interactions. However, it does capture some intermediate-range dispersionlike binding through the behavior of its exchange functional, which can be viewed as an error cancellation between the exchange and correlation terms [30]. This dispersionlike behavior contributes to its improved performance relative to PBE.

Table I also shows that the addition of dispersion to the PBE or B86bPBE functionals leads (in most cases) to volume contraction, causing the static cell volumes to become smaller than the experimental volumes. Inclusion of thermal expansion now improves the agreement with the room-temperature reference data, as would be expected for an accurate DF method. Overall, pairing PBE and B86bPBE with any of the D3, D3(BJ), and XDM dispersion models results in good agreement between the computed V_{th} data and the experimental unit-cell volumes. The MEs and MAEs are comparable to those obtained with PBEsol in the absence of a dispersion correction, similar to what was seen in previous work for ionic solids [45].

The TS dispersion correction results in significantly greater cell contraction than obtained with D3, D3(BJ), or XDM. This is expected since TS gives atomic C_6 dispersion coefficients for metals that are typically greater than or equal to their neutral free-atom reference values [109]. Consequently, the TS dispersion coefficients are much larger than those obtained using D3 or XDM [109]. Overestimation of the dispersion coefficients results in excessive cell contraction and systematic underestimation of V_{th}. Thus, PBE-TS exhibits the largest MAEs and most negative MEs obtained with any of the DC-DFs considered.

Lastly, we compare the performance of the PAW and NAO implementations of the uncorrected and XDM-corrected DFs. Ideally, both implementations should yield identical results. However, in practice the NAO results may be adversely affected by basis-set incompleteness, while the PAW results may show significant errors, particularly at high compression, due to the replacement of core electrons with pseudopotentials. For the dispersion-uncorrected functionals, the agreement between the two codes is excellent. For the XDM-corrected functionals, the agreement between QE and FHI-aims is again excellent for the IM07 set. However, for the EM11 set (with the exceptions of Mo, Ta, and W), the FHI-aims XDM implementation tends to give significantly smaller cell volumes, and hence larger dispersion-induced contraction, than obtained with QE. The consistency of the uncorrected GGA results rules out any basis-set incompleteness.

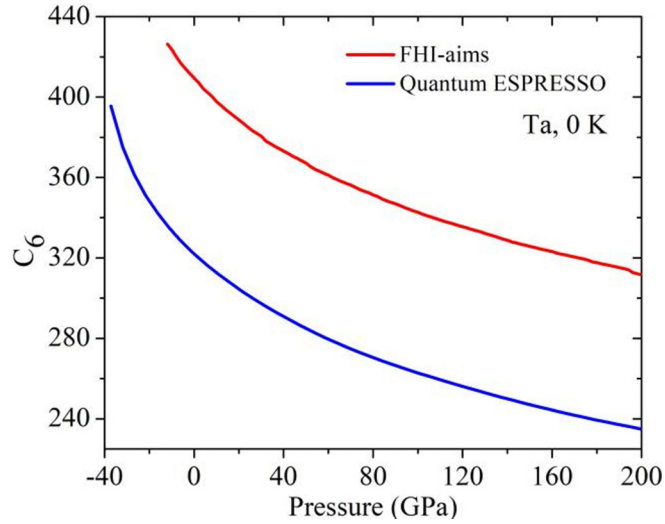

FIG. 2. Change in homoatomic XDM C_6 dispersion coefficient (in atomic units) for Ta as a function of applied pressure. Results were obtained using B86bPBE-XDM with either the all-electron code FHI-aims or the plane-wave/pseudopotential code QUANTUM ESPRESSO.

We therefore conjecture that this difference arises from contributions of the core electrons to the dispersion coefficients that will be captured in the all-electron FHI-aims implementation, but not in the QE pseudopotential implementation of XDM. Indeed, the QE calculations tend to provide somewhat smaller C_6 dispersion coefficients than the FHI-aims results, by 26% on average for the 11 elemental metals. As exemplified in Fig. 2, the difference in dispersion coefficients increases with applied pressure, as the spatial extent of the valence region decreases and the atomic cores represent a proportionally larger amount of the cell volume.

C. Bulk moduli

Table II displays error statistics for the computed bulk moduli (B_{th} at 293 K) obtained for the EM11 and IM07 benchmarks; results using the static bulk moduli (B_0) are also displayed in parentheses. The bulk moduli obtained with the dispersion-uncorrected GGA functionals follow a general trend of B86bPBE < PBE ≪ PBEsol. This is the reverse of the cell-volume trend, since smaller cells typically have stronger bonding and a higher bulk modulus, while larger cells tend to have weaker bonding and a lower bulk modulus.

The bulk modulus is known to have a significant dependence on temperature [110–112]. With an accurate DF model, static 0 K predictions are expected to overestimate the bulk modulus, while thermal correction lowers the computed values and improves agreement with experiment. This is the case with PBEsol, although the bulk moduli remain slightly overestimated, even with inclusion of thermal effects. Similarly, with the dispersion-corrected functionals, the computed static bulk moduli are significantly higher than the room-temperature experimental values. This leads to a consistent reduction in the MEs after correcting for temperature effects.

Of the dispersion-corrected DFs, PBE-TS shows the poorest performance, consistently overestimating the bulk moduli,

TABLE II. Mean errors (MEs) and mean absolute errors (MAEs) in bulk moduli, in GPa, computed with selected density functionals and dispersion corrections. The results correspond to the thermally corrected values (B_{th}), while the static values (B_0) are given in parentheses. Errors are shown for the EM11 and IM07 benchmarks separately, as well as for the combined data set.

		EM11				IM07				Combined			
	Method	ME		MAE		ME		MAE		ME		MAE	
QE	PBEsol	5.3	(18.6)	15.6	(23.9)	5.7	(18.1)	14.1	(23.8)	5.5	(18.4)	15.0	(23.9)
	PBE	−15.8	(−2.4)	18.9	(13.4)	−5.0	(5.1)	19.3	(20.7)	−11.6	(0.5)	19.0	(16.2)
	B86bPBE	−22.5	(−1.3)	25.2	(10.8)	−5.9	(2.7)	20.3	(20.4)	−16.1	(0.3)	23.3	(14.5)
	PBE-D3	−0.2	(13.4)	13.0	(16.8)	4.7	(12.8)	19.4	(20.8)	1.7	(13.2)	15.5	(18.4)
	PBE-D3BJ	−1.8	(16.2)	11.0	(17.6)	6.8	(15.5)	19.2	(22.8)	1.6	(16.0)	14.1	(19.6)
	PBE-XDM	−9.0	(27.8)	20.1	(29.1)	4.6	(29.0)	25.7	(32.6)	−3.8	(28.3)	22.3	(30.5)
	B86bPBE-XDM	−8.2	(25.1)	22.2	(28.5)	−2.1	(23.8)	24.9	(28.8)	−5.8	(24.6)	23.2	(28.6)
FHI-aims	PBEsol	9.4	(26.5)	13.0	(26.5)	7.4	(12.9)	18.6	(20.4)	8.6	(21.2)	15.2	(24.1)
	PBE	−14.3	(0.4)	19.5	(14.7)	−5.0	(1.8)	20.4	(19.4)	−10.7	(0.9)	19.8	(16.6)
	B86bPBE	−19.4	(−3.9)	22.1	(14.8)	−7.9	(0.3)	19.3	(20.2)	−14.9	(−2.2)	21.0	(16.9)
	PBE-TS	25.8	(39.7)	38.9	(42.8)	15.3	(24.4)	22.7	(30.2)	21.7	(33.8)	32.6	(37.9)
	PBE-XDM	3.9	(31.4)	23.5	(31.7)	1.2	(17.4)	14.8	(22.2)	2.9	(25.9)	20.1	(28.0)
	B86bPBE-XDM	−4.8	(25.6)	18.1	(27.4)	−0.7	(14.8)	14.8	(20.2)	−3.2	(21.4)	16.8	(24.6)

as expected from its underestimation of the cell volumes. We suggest that it should not be used in the description of elemental metals. Also consistent with the volume results, PBE-D3 and PBE-D3(BJ) give the lowest MAEs for the bulk moduli with the PAW implementation, while PBE-XDM and B86bPBE-XDM give the lowest MAEs with the NAO implementation. As noted previously, the discrepancies in the performance of the XDM-corrected functionals when switching between the PAW and NAO methods may be due to the difference in the treatment of the core electrons.

The performance of various (DC-)DFs is illustrated in terms of the correlation of errors in V_{th} and B_{th} in Fig. 3 for the combined benchmark of 18 metals. As one would expect, there is an almost linear correlation between the MEs in V_{th} and in B_{th}. The figure shows the strong underbinding of uncorrected PBE and B86bPBE and the strong overbinding of PBE-TS. Overall, PBEsol, PBE-D3, PBE-D3BJ, PBE-XDM, and B86bPBE-XDM show minimal systematic errors, with MEs near zero for both quantities. PBEsol, PBE-D3, PBE-D3BJ, and the FHI-aims implementation of B86bPBE-XDM also give the lowest MAEs.

D. Pressure derivatives of the bulk moduli

The pressure derivative of the bulk modulus (B′) is an integral part of the EOS and has great significance in high-pressure physics. In geoscience it is used as a parameter required for the accurate inversion of seismic data into texture, composition, and structure, as well as for determining the thermal profile of the Earth's interior. B′ also has a global correlation with the bonding and interstitial electron density of a material [113]. In practice, B′ can be extracted from the $P(V)$ isotherm, a direct measurement of the pressure evolution of the sonic velocity, or by taking the slope of the shock velocity versus particle velocity curve [113]. Due to the significance of B′ in the description of some thermophysical properties, such as the thermal expansivity and the heat capacity of a material [114], it is desirable to benchmark the performance of various DFs and DC-DFs for its prediction.

Error statistics for the computed B_0' and B_{th}' values are collected in Table III. In contrast to the volume and bulk modulus results, there is minimal change in the MAEs with the choice of functional and/or dispersion correction. Additionally, the application of thermal corrections to the cold compression EOS tends to increase the pressure derivative of the bulk modulus, consequently increasing the MEs and MAEs obtained with all methods. This leads to the unfortunate conclusion that the computed B_0' is a better approximation to the room-temperature experimental data than is B_{th}'. This may be due to a breakdown in the simple and computationally expedient Debye approximation used here for the thermal correction, or some other systematic error in the DF results.

E. Phase transitions

Pressure-induced phase transition is a common phenomenon in materials physics. At ambient conditions, the relative stability between two phases is determined by the relative static energy. The phase with lower static energy is considered more energetically stable. For materials subjected to external pressure, the relative stability metric is modified to include the work done on the system through volume contraction, known as the PV work. At finite temperature, the system is described in terms of its free energy,

$$G = E + PV + F_{\text{vib}} = E - V\left(\frac{dE}{dV}\right) + F_{\text{vib}}. \quad (11)$$

For competing phases of the same material, the phase with the lowest enthalpy at a given pressure is considered the most stable at 0 K. At finite temperatures, the F_{vib} is added and the phase with the lowest free energy is most stable.

In this section, we consider a new benchmark set (PT05) composed of five intermetallic compounds with known experimental phase-transition pressures. The two competing phases of each of these compounds were compressed within the NAO formalism using FHI-aims and the free energies of each evaluated at finite temperature to determine the transition pressure (P_c). Figure 4 shows the phase-transition EOS of

TABLE III. Mean errors (MEs) and mean absolute errors (MAEs) in the pressure derivatives of the bulk moduli, computed with selected density functionals and dispersion corrections. The results correspond to the thermally corrected values ($B'_{\rm th}$), while the static values (B'_0) are given in parentheses. Errors are shown for the EM11 and IM07 benchmarks separately, as well as for the combined data set.

		EM11				IM07				Combined			
	Method	ME		MAE		ME		MAE		ME		MAE	
QE	PBEsol	0.32	(0.27)	0.72	(0.37)	0.35	(−0.33)	0.97	(0.81)	0.34	(0.04)	0.82	(0.54)
	PBE	0.50	(0.32)	0.59	(0.42)	−0.04	(−0.26)	0.72	(0.80)	0.29	(0.09)	0.64	(0.57)
	B86bPBE	0.44	(0.36)	0.52	(0.43)	0.12	(−0.24)	0.74	(0.83)	0.32	(0.13)	0.60	(0.59)
	PBE-D3	0.53	(0.36)	0.61	(0.45)	0.02	(−0.20)	0.85	(0.83)	0.33	(0.14)	0.70	(0.60)
	PBE-D3BJ	0.47	(0.26)	0.53	(0.36)	−0.18	(−0.32)	0.89	(0.85)	0.22	(0.03)	0.67	(0.55)
	PBE-XDM	0.49	(0.23)	0.53	(0.27)	0.39	(−0.38)	0.67	(0.86)	0.45	(−0.01)	0.59	(0.50)
	B86bPBE-XDM	0.41	(0.22)	0.53	(0.30)	0.22	(−0.35)	0.89	(0.84)	0.34	(−0.00)	0.67	(0.51)
FHI-aims	PBEsol	0.35	(0.15)	0.36	(0.34)	0.21	(−0.12)	1.07	(0.98)	0.30	(0.04)	0.64	(0.59)
	PBE	0.55	(0.34)	0.55	(0.36)	−0.07	(−0.23)	0.82	(0.89)	0.31	(0.12)	0.66	(0.57)
	B86bPBE	0.46	(0.28)	0.46	(0.34)	−0.24	(−0.26)	1.00	(0.87)	0.19	(0.07)	0.67	(0.55)
	PBE-TS	0.20	(0.15)	0.35	(0.39)	0.42	(0.22)	1.24	(1.18)	0.29	(0.18)	0.70	(0.70)
	PBE-XDM	0.18	(0.04)	0.63	(0.40)	−0.07	(−0.40)	0.78	(0.78)	0.08	(−0.13)	0.69	(0.55)
	B86bPBE-XDM	0.40	(0.19)	0.57	(0.30)	−0.03	(−0.37)	0.70	(0.82)	0.23	(−0.03)	0.62	(0.50)

$SrAl_2$ as an illustrative example, while Table IV shows the computed phase-transition pressures of all five compounds across the various levels of theory used.

As shown in Table IV, the MAE of the dispersion-uncorrected GGAs in predicting P_c follows the trend of PBEsol < PBE < B86bPBE, which is consistent with the MAE trend in $V_{\rm th}$ (see Table I). This is not surprising since the quality of the predicted transition pressure is expected to improve with more accurate cell volumes. Pairing the PBE and B86bPBE DFs with dispersion corrections yields the trend PBE-XDM < B86bPBE-XDM < PBE-TS for the P_c MAEs. PBE-TS is again not recommended and is the only method that obtains negative transition pressures (see Fig. 4), indicating an incorrect stability ranking of the two phases in the absence of applied pressure.

Across all methods considered, PBE-XDM and B86bPBE-XDM provide the best performance in predicting the phase-transition pressure within the PT05 benchmark set. However, the MAEs remain very large relative to the transition pressures themselves, and individual errors can be in excess of 10 GPa with even the best-performing functionals. This may be due to a combination of limitations of the computational treatment and uncertainties in the experimental data, since the phase change can span a range of applied pressures during compression. The range of applied pressures for which phase transition is observed depends on the method used for the experimental compression of the materials and the phase-transition rate [115].

IV. DISCUSSION

Dispersion arises from interaction of instantaneous dipole (and higher-order multipole) moments of atoms due to fluctuations in their electron densities. At both equilibrium and expanded geometries, dispersion plays an important role in the accurate description of molecular crystals and other solid-state systems. From second-order perturbation theory [116], the dispersion energy takes the form of an asymptotic series expansion in the interatomic distance, R:

$$E_{\rm disp} = -\frac{C_6}{R^6} - \frac{C_8}{R^8} - \frac{C_{10}}{R^{10}} - \cdots, \tag{12}$$

with higher-order terms having increasingly minor contributions. The number of terms included in this expansion depends on the particular dispersion correction, with TS including only the leading-order C_6 term, D3 including the C_6 and C_8 terms, and XDM including C_6, C_8, and C_{10}. In practice, the dispersion

TABLE IV. Room-temperature phase-transition pressures (P_c), in GPa, computed for the PT05 benchmark set using FHI-aims. Experimental reference data [82–85,88] at 293 K are also shown.

	GGA			GGA+Dispersion			
Material	PBEsol	PBE	B86bPBE	PBE-TS	PBE-XDM	B86bPBE-XDM	Expt.
Na_3Bi	4.85	6.45	7.00	3.90	0.82	0.80	1.00
$SrAl_2$	0.20	1.95	2.84	−3.26	1.00	0.88	1.80
$ScGa_2$	21.62	21.82	21.50	−1.06	19.62	19.56	7.70
LiCd	3.00	4.50	5.50	−0.82	5.00	2.57	11.00
$AuAl_2$	14.50	16.00	17.40	11.00	10.80	11.00	12.50
ME	2.03	3.34	4.05	−4.85	0.65	0.16	
MAE	5.87	5.94	6.25	6.01	4.12	4.58	

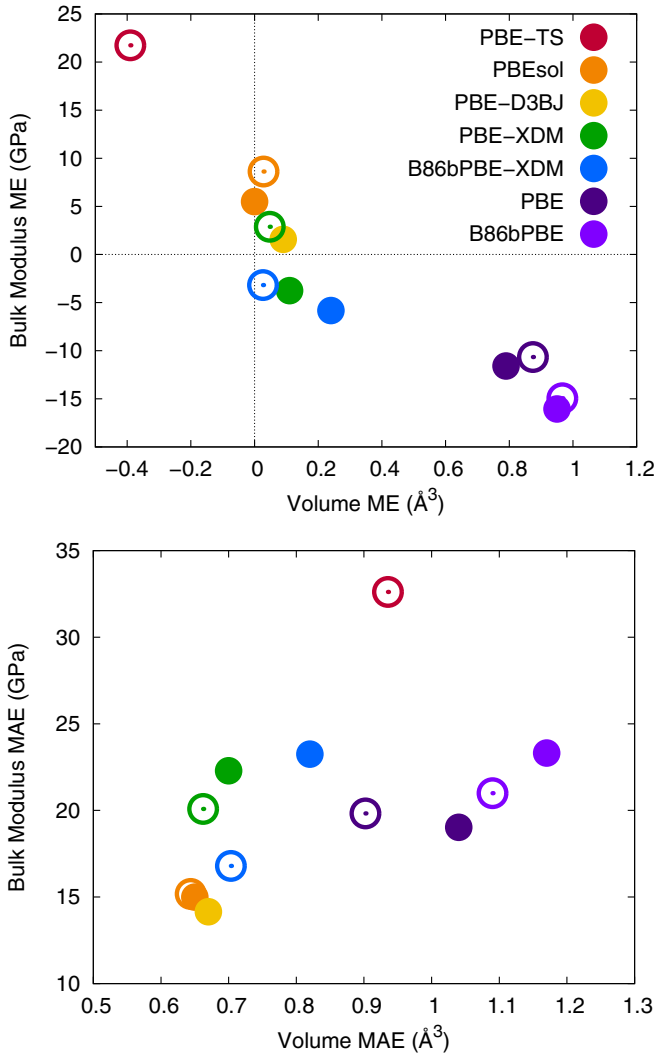

FIG. 3. Correlation of MEs (top) and MAEs (bottom) in V_{th} and B_{th} for the combined EM11 and IM07 benchmark sets. Solid points are from QUANTUM ESPRESSO and open points are from FHI-aims. Due to the high degree of similarity in the PBE-D3 and PBE-D3(BJ) results, only the latter are shown.

energy is damped (to zero or a small, constant value [30]) for short internuclear separations.

Given that dispersion interactions are inherently long-range, it is perhaps counterintuitive to readers that they should also matter for bulk metals. For compressed metals, bonded atoms become closer than their equilibrium separations, where the dispersion energy is almost completely damped. However, long-range dispersion forces are still present between atoms and their more distant neighbors within the periodic lattice. While screening by surrounding atoms or molecules can reduce the magnitude of the dispersion energy, these interactions can still be felt between pairs of atoms separated by up to a few tens of angstroms.

To illustrate why dispersion is important across the whole EOS, we consider the two-dimensional crystal lattice shown in Fig. 5 as a model system. This model has a square unit cell of length a that is replicated in both the x and y directions. The blue lines indicate the approximate x-distance from a point at

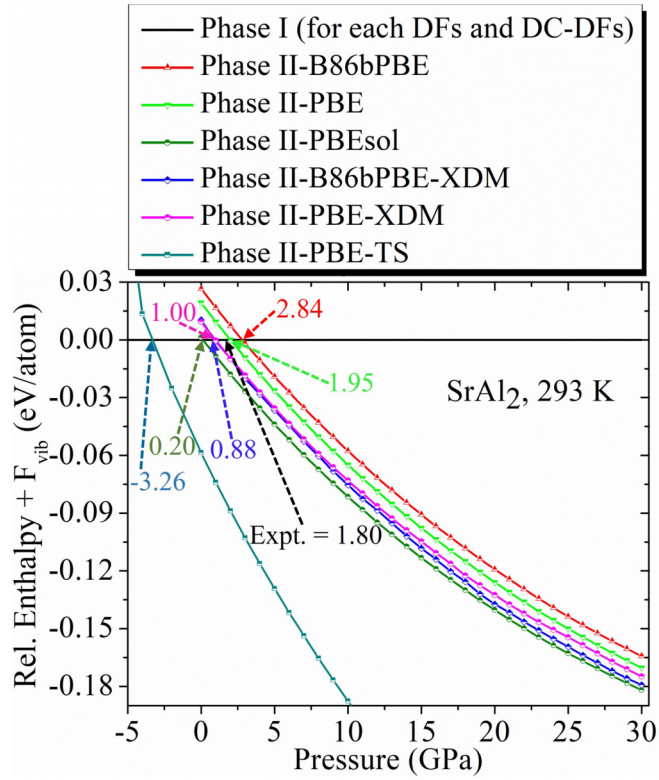

FIG. 4. Room-temperature EOS for $SrAl_2$ computed using different (DC-)DFs within the NAO formalism. The experimental data are from Ref. [83].

the center of the image at which dispersion interactions would become significantly damped. Let us first consider the left panel, corresponding to ambient conditions. Since atoms A and B are nearest neighbors, the dispersion energy between them is highly damped and their interactions are well described by the base density functional. Conversely, dispersion interactions between atoms A and B′ (and between atoms A′ and B) would be undamped, and these energy contributions must be included via the dispersion correction.

To quantify the length scales under discussion, we consider the sum of van der Waals radii that appear in the XDM damping function [54] using the B86bPBE-XDM results at ambient pressure. For the 3*d* transition metals, this sum of radii decreases from 3.86 to 3.70 Å across the row from Fe to Zn. As expected, the sums of vdW radii are larger for the

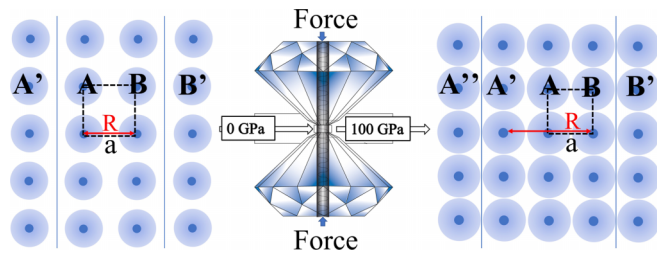

FIG. 5. Illustration of the geometric changes in a simple solid at ambient conditions (left) and upon compression (right). The dark blue balls represent atomic nuclei and the light blue balls represent the electron clouds around each atom.

4*d* and 5*d* metals; they are 3.9–4.0 Å for Ag, Pt, and Au and 4.1–4.2 Å for W, Mo, and Ta. The variations between early- and late-group transition metals are due to the increased effective nuclear charge. Overall, the sums of vdW radii are roughly 4 Å for all metals considered. This means that the dispersion energy will be damped to half its value when a pair of metal atoms are separated by this distance. We can then use 4 Å as an approximate length scale at which the dispersion interactions become highly damped in Fig. 5. This can be contrasted with the metal-metal bond lengths in these systems, which range from 2.4 to 2.9 Å at ambient pressure.

Now we consider the right panel of Fig. 5, which illustrates the situation when pressure is applied to the system, for example using a diamond anvil cell. This reduces the lattice constant such that a becomes much less than the equilibrium bond length (R in the figure). This causes the A-B′ and A′-B interactions to move into the short-range region where they are damped. However, we must still account for long-range dispersion interactions for A″-B and A′-B′. At high pressure, there are more neighbors within a given radius of a reference atom that can contribute to the dispersion energy, and its magnitude therefore increases with pressure. Thus, dispersion can be important in the description of metals at ambient conditions and under compression, as it is in the description of molecular solids.

V. CONCLUSION

In this article, we studied the performance of selected density functionals and post-SCF dispersion corrections for the description of compressed elemental metals and intermetallic compounds relative to high-pressure experimental data. Four properties were considered: the unit-cell volume, the bulk modulus, the pressure derivative of the bulk modulus, and phase-transition pressures.

Thermal expansion is important when comparing with experiment as DF calculations give by default the static (0 K) energy and volume, while experiments are performed at finite temperature (of 293 K or higher). Correcting for thermal effects leads to a reduction in the errors for computed volumes and bulk moduli with most functionals considered. The simple Debye model used here is a very appealing alternative to computationally expensive thermal-correction methods such as the harmonic or quasiharmonic approximations. However, the Debye method may not be as accurate and is perhaps one source of error contributing to the poor predictions of B'_{th} and some phase-transition pressures.

The dispersion models that we recommend through this study are D3, D3(BJ), and XDM. We suggest that the TS dispersion model should not be used for the study of elemental metals and intermetallic compounds as the model overestimates dispersion effects in these systems. Additionally, PBEsol without any dispersion correction generally gives low errors for prediction of volumes and bulk moduli due to the behavior of its enhancement factor and systematic error cancellation between exchange and the lack of dispersion correlation. Overall, PBE-D3 and PBE-D3(BJ) with QUANTUM ESPRESSO, PBE-XDM and B86bPBE-XDM with FHI-aims, and PBEsol (with both codes) give the best performance of the methods considered.

There is excellent agreement between the plane wave and NAO implementations of PBEsol and other GGA functionals. For XDM, the NAO implementation gives larger dispersion coefficients than obtained with the PAW method, leading to greater volume contraction for many of the elemental metals and improved agreement with experiment. This implies that dispersion contributions from the core electrons are not negligible in metals.

Past studies have demonstrated that dispersion is important in the description of both molecular and ionic solids under ambient conditions. However, whether dispersion matters or not is a question that is routinely asked by scientists studying materials under extreme conditions. The present work establishes that we should include long-range dispersion interactions when describing metals both at ambient conditions and under compression, and it is important to carefully choose an appropriate dispersion model.

ACKNOWLEDGMENTS

This research was funded by the Natural Sciences and Engineering Research Council of Canada (NSERC). The authors are grateful to the Digital Research Alliance of Canada for computational resources.

[1] J.-P. Poirier, *Introduction to the Physics of the Earth's Interior* (Cambridge University Press, Cambridge, 2000).
[2] J. Lindl, Phys. Plasmas **2**, 3933 (1995).
[3] A. Dewaele, P. Loubeyre, and M. Mezouar, Phys. Rev. B **70**, 094112 (2004).
[4] A. Dewaele, M. Torrent, P. Loubeyre, and M. Mezouar, Phys. Rev. B **78**, 104102 (2008).
[5] R. M. Martin, *Electronic Structure: Basic Theory and Practical Methods* (Cambridge University Press, 2020), p. 16.
[6] P. Hohenberg and W. Kohn, Phys. Rev. **136**, B864 (1964).
[7] W. Kohn and L. J. Sham, Phys. Rev. **140**, A1133 (1965).
[8] J. P. Perdew, K. Burke, and M. Ernzerhof, Phys. Rev. Lett. **77**, 3865 (1996).
[9] A. Becke, J. Chem. Phys. **85**, 7184 (1986).
[10] C. Lee, W. Yang, and R. G. Parr, Phys. Rev. B **37**, 785 (1988).
[11] A. D. Becke, Phys. Rev. A **38**, 3098 (1988).
[12] J. P. Perdew, A. Ruzsinszky, G. I. Csonka, O. A. Vydrov, G. E. Scuseria, L. A. Constantin, X. Zhou, and K. Burke, Phys. Rev. Lett. **100**, 136406 (2008).
[13] A. D. Becke and M. R. Roussel, Phys. Rev. A **39**, 3761 (1989).
[14] J. Tao, J. P. Perdew, V. N. Staroverov, and G. E. Scuseria, Phys. Rev. Lett. **91**, 146401 (2003).
[15] Y. Zhao and D. G. Truhlar, J. Chem. Phys. **125**, 194101 (2006).
[16] J. P. Perdew, A. Ruzsinszky, G. I. Csonka, L. A. Constantin, and J. Sun, Phys. Rev. Lett. **103**, 026403 (2009).
[17] J. Sun, A. Ruzsinszky, and J. P. Perdew, Phys. Rev. Lett. **115**, 036402 (2015).

[18] J. W. Furness, A. D. Kaplan, J. Ning, J. P. Perdew, and J. Sun, J. Phys. Chem. Lett. **11**, 8208 (2020).
[19] A. D. Becke, J. Chem. Phys. **98**, 1372 (1993).
[20] A. D. Becke, J. Chem. Phys. **98**, 5648 (1993).
[21] J. Heyd, G. E. Scuseria, and M. Ernzerhof, J. Chem. Phys. **118**, 8207 (2003).
[22] C. Adamo and V. Barone, J. Chem. Phys. **110**, 6158 (1999).
[23] V. Ozoliņš and M. Körling, Phys. Rev. B **48**, 18304 (1993).
[24] G. I. Csonka, J. P. Perdew, A. Ruzsinszky, P. H. T. Philipsen, S. Lebègue, J. Paier, O. A. Vydrov, and J. G. Ángyán, Phys. Rev. B **79**, 155107 (2009).
[25] K. Lejaeghere, V. Van Speybroeck, G. Van Oost, and S. Cottenier, Crit. Rev. Solid State Mater. Sci. **39**, 1 (2014).
[26] F. London, Z. Phys. **63**, 245 (1930).
[27] A. Otero de la Roza and G. A. DiLabio, *Non-covalent Interactions in Quantum Chemistry and Physics: Theory and Applications* (Elsevier, Amsterdam, 2017).
[28] S. Grimme, A. Hansen, J. G. Brandenburg, and C. Bannwarth, Chem. Rev. **116**, 5105 (2016).
[29] J. Hermann, R. A. DiStasio Jr., and A. Tkatchenko, Chem. Rev. **117**, 4714 (2017).
[30] A. J. Price, K. R. Bryenton, and E. R. Johnson, J. Chem. Phys. **154**, 230902 (2021).
[31] M. Micoulaut, A. Piarristeguy, H. Flores-Ruiz, and A. Pradel, Phys. Rev. B **96**, 184204 (2017).
[32] F. Della Pia, A. Zen, D. Alfè, and A. Michaelides, J. Chem. Phys. **157**, 134701 (2022).
[33] J. Moellmann and S. Grimme, Phys. Chem. Chem. Phys. **12**, 8500 (2010).
[34] M. A. Neumann, F. J. J. Leusen, and J. Kendrick, Angew. Chem. Int. Ed. **47**, 2427 (2008).
[35] A. Asmadi, M. A. Neumann, J. Kendrick, P. Girard, M.-A. Perrin, and F. J. J. Leusen, J. Phys. Chem. B **113**, 16303 (2009).
[36] W. Liu, A. Tkatchenko, and M. Scheffler, Acc. Chem. Res. **47**, 3369 (2014).
[37] M. S. Christian, A. Otero-de-la-Roza, and E. R. Johnson, J. Chem. Theor. Comput. **12**, 3305 (2016).
[38] M. Kolář, T. Kubař, and P. Hobza, J. Phys. Chem. B **115**, 8038 (2011).
[39] T. Risthaus and S. Grimme, J. Chem. Theor. Comput. **9**, 1580 (2013).
[40] A. Otero-de-la-Roza and E. R. Johnson, J. Chem. Phys. **137**, 054103 (2012).
[41] A. M. Reilly and A. Tkatchenko, J. Chem. Phys. **139**, 024705 (2013).
[42] S. A. Tawfik, T. Gould, C. Stampfl, and M. J. Ford, Phys. Rev. Mater. **2**, 034005 (2018).
[43] W. Ouyang, I. Azuri, D. Mandelli, A. Tkatchenko, L. Kronik, M. Urbakh, and O. Hod, J. Chem. Theor. Comput. **16**, 666 (2020).
[44] A. Otero-de-la-Roza, L. M. LeBlanc, and E. R. Johnson, J. Phys. Chem. Lett. **11**, 2298 (2020).
[45] A. Otero-de-la-Roza and E. R. Johnson, J. Chem. Phys. **153**, 054121 (2020).
[46] S. Jana, H. Myneni, S. Śmiga, L. A. Constantin, and P. Samal, J. Chem. Phys. **155**, 114102 (2021).
[47] A. Tkatchenko and M. Scheffler, Phys. Rev. Lett. **102**, 073005 (2009).
[48] S. Grimme, J. Comput. Chem. **27**, 1787 (2006).
[49] S. Grimme, J. Antony, S. Ehrlich, and H. Krieg, J. Chem. Phys. **132**, 154104 (2010).
[50] S. Grimme, S. Ehrlich, and L. Goerigk, J. Comput. Chem. **32**, 1456 (2011).
[51] E. Caldeweyher, S. Ehlert, A. Hansen, H. Neugebauer, S. Spicher, C. Bannwarth, and S. Grimme, J. Chem. Phys. **150**, 154122 (2019).
[52] E. Caldeweyher, J.-M. Mewes, S. Ehlert, and S. Grimme, Phys. Chem. Chem. Phys. **22**, 8499 (2020).
[53] A. D. Becke and E. R. Johnson, J. Chem. Phys. **127**, 154108 (2007).
[54] E. R. Johnson, in *Non-covalent Interactions in Quantum Chemistry and Physics*, edited by A. Otero-de-la-Roza and G. A. DiLabio (Elsevier, Amsterdam, 2017), Chap. 5, pp. 169–194.
[55] A. Tkatchenko, R. A. DiStasio, Jr., R. Car, and M. Scheffler, Phys. Rev. Lett. **108**, 236402 (2012).
[56] A. Ambrosetti, A. M. Reilly, R. A. DiStasio, Jr., and A. Tkatchenko, J. Chem. Phys. **140**, 18A508 (2014).
[57] T. Gould, S. Lebegue, J. G. Ángyán, and T. Bučko, J. Chem. Theor. Comput. **12**, 5920 (2016).
[58] M. Kim, W. J. Kim, T. Gould, E. K. Lee, S. Lebegue, and H. Kim, J. Am. Chem. Soc. **142**, 2346 (2020).
[59] M. Dion, H. Rydberg, E. Schröder, D. C. Langreth, and B. I. Lundqvist, Phys. Rev. Lett. **92**, 246401 (2004).
[60] G. Román-Pérez and J. M. Soler, Phys. Rev. Lett. **103**, 096102 (2009).
[61] K. Lee, É. D. Murray, L. Kong, B. I. Lundqvist, and D. C. Langreth, Phys. Rev. B **82**, 081101(R) (2010).
[62] O. A. Vydrov and T. Van Voorhis, J. Chem. Phys. **133**, 244103 (2010).
[63] R. Sabatini, T. Gorni, and S. de Gironcoli, Phys. Rev. B **87**, 041108(R) (2013).
[64] L. Gráfová, M. Pitoňák, J. Řezáč, and P. Hobza, J. Chem. Theor. Comput. **6**, 2365 (2010).
[65] J. Řezáč, K. E. Riley, and P. Hobza, J. Chem. Theor. Comput. **7**, 3466 (2011).
[66] T. Gould, E. R. Johnson, and S. A. Tawfik, Beilstein J. Org. Chem. **14**, 1181 (2018).
[67] A. Mazurek, Ł. Szeleszczuk, and D. M. Pisklak, Molecules **25**, 1584 (2020).
[68] W. Wang, H. Li, Q. Liu, F. Liu, and Z. Liu, Phys. Status Solidi B **258**, 2000329 (2021).
[69] Y. Wang, D. Chen, and X. Zhang, Phys. Rev. Lett. **84**, 3220 (2000).
[70] L. K. Magad-Weiss, A. A. Adeleke, E. Greenberg, V. B. Prakapenka, Y. Yao, and E. Stavrou, Phys. Rev. B **103**, 014101 (2021).
[71] A. A. Adeleke and Y. Yao, J. Chem. Phys. **148**, 104503 (2018).
[72] A. A. Adeleke, E. E. Jossou, N. U. Ukoji, A. O. Adeniyi, and P. O. Egbele, ACS Omega **5**, 26786 (2020).
[73] P. E. Blöchl, Phys. Rev. B **50**, 17953 (1994).
[74] V. Blum, R. Gehrke, F. Hanke, P. Havu, V. Havu, X. Ren, K. Reuter, and M. Scheffler, Comput. Phys. Commun. **180**, 2175 (2009).
[75] P. Giannozzi, O. Andreussi, T. Brumme, O. Bunau, M. B. Nardelli, M. Calandra, R. Car, C. Cavazzoni, D. Ceresoli, M. Cococcioni *et al.*, J. Phys.: Condens. Matter **29**, 465901 (2017).
[76] M. De La Pierre, R. Orlando, L. Maschio, K. Doll, P. Ugliengo, and R. Dovesi, J. Comput. Chem. **32**, 1775 (2011).

[77] E. R. Johnson and A. D. Becke, J. Chem. Phys. **124**, 174104 (2006).

[78] A. J. A. Price, A. Otero-de-la-Roza, and E. R. Johnson, Chem. Sci. **14**, 1252 (2023).

[79] See Supplemental Material at http://link.aps.org/supplemental/10.1103/PhysRevB.107.064101 for computational settings, plots of the equations of state, and full data tables.

[80] A. Otero-de-la-Roza, L. M. LeBlanc, and E. R. Johnson, Phys. Chem. Chem. Phys. **22**, 8266 (2020).

[81] H. Giefers and M. Nicol, J. Alloys Compd. **422**, 132 (2006).

[82] A. B. Garg, A. K. Verma, V. Vijayakumar, R. S. Rao, and B. K. Godwal, Phys. Rev. B **72**, 024112 (2005).

[83] S. Kal, E. Stoyanov, J.-P. Belieres, T. L. Groy, R. Norrestam, and U. Häussermann, J. Solid State Chem. **181**, 3016 (2008).

[84] G. Cordier, E. Czech, and H. Schäfer, Z. Naturforsch. B **37**, 1442 (1982).

[85] Z.-J. Fu, L.-J. Jia, J.-H. Xia, K. Tang, Z.-H. Li, X.-W. Sun, and Q.-F. Chen, Z. Naturforsch. A **70**, 1007 (2015).

[86] A. B. Garg, P. Modak, and V. Vijayakumar, J. Appl. Phys. **109**, 083531 (2011).

[87] B. K. Godwal, S. Speziale, S. M. Clark, J. Yan, and R. Jeanloz, Phys. Rev. B **78**, 094107 (2008).

[88] R. Demchyna, S. Leoni, H. Rosner, and U. Schwarz, Z. Kristallog.-Cryst. Mater. **221**, 420 (2006).

[89] S.-L. Shang, Y. Wang, D. Kim, and Z.-K. Liu, Comput. Mater. Sci. **47**, 1040 (2010).

[90] P. Vinet, J. Ferrante, J. H. Rose, and J. R. Smith, J. Geophys. Res. Solid Earth **92**, 9319 (1987).

[91] F. D. Murnaghan, Am. J. Math. **59**, 235 (1937).

[92] F. Birch, Phys. Rev. **71**, 809 (1947).

[93] T. Katsura and Y. Tange, Minerals **9**, 745 (2019).

[94] P. J. J. R. Vinet, J. Ferrante, J. R. Smith, and J. H. Rose, J. Phys. C **19**, L467 (1986).

[95] P. Vinet, J. R. Smith, J. Ferrante, and J. H. Rose, Phys. Rev. B **35**, 1945 (1987).

[96] O. L. Anderson, *Equations of State of Solids for Geophysics and Ceramic Science* (Oxford University Press on Demand, 1995), p. 31.

[97] Y. Wang, R. Ahuja, and B. Johansson, Int. J. Quantum Chem. **96**, 501 (2004).

[98] V. L. Moruzzi, J. F. Janak, and K. Schwarz, Phys. Rev. B **37**, 790 (1988).

[99] H. C. Herper, E. Hoffmann, and P. Entel, Phys. Rev. B **60**, 3839 (1999).

[100] K. R. Bryenton, A. A. Adeleke, S. G. Dale, and E. R. Johnson, Wiley Interdiscip. Rev. Comp. Mol. Sci. e1631 (2022).

[101] M. Cococcioni and S. de Gironcoli, Phys. Rev. B **71**, 035105 (2005).

[102] Y. S. Mohammed, Y. Yan, H. Wang, K. Li, and X. Du, J. Magn. Magn. Mater. **322**, 653 (2010).

[103] N. V. Solomatova and P. D. Asimow, Phys. Chem. Miner. **45**, 293 (2018).

[104] D. J. Lacks and R. G. Gordon, Phys. Rev. A **47**, 4681 (1993).

[105] Y. Zhang, W. Pan, and W. Yang, J. Chem. Phys. **107**, 7921 (1997).

[106] E. D. Murray, K. Lee, and D. C. Langreth, J. Chem. Theor. Comput. **5**, 2754 (2009).

[107] M. J. Gillan, J. Chem. Phys. **141**, 224106 (2014).

[108] P. Haas, F. Tran, and P. Blaha, Phys. Rev. B **79**, 085104 (2009).

[109] J. Tao, H. Tang, A. Patra, P. Bhattarai, and J. P. Perdew, Phys. Rev. B **97**, 165403 (2018).

[110] D. B. Sirdeshmukh, L. Sirdeshmukh, and K. Subhadra, *Alkali Halides: A Handbook of Physical Properties* (Springer Science & Business Media, 2001), Vol. 49.

[111] K.-O. Park and J. M. Sivertsen, J. Am. Ceram. Soc. **60**, 537 (1977).

[112] Q. He and Z.-T. Yan, Phys. Status Solidi B **223**, 767 (2001).

[113] S. Raju, E. Mohandas, and V. S. Raghunathan, J. Phys. Chem. Solids **58**, 1367 (1997).

[114] H. Li, L. Xu, and C.-Q. Liu, J. Geophys. Res. Solid Earth **110** (2005).

[115] R. Etters, K. Kobashi, and V. Chandrasekharan, in *Shock Waves in Condensed Matter 1983*, edited by J. R. Asay, R. A. Graham, and G. K. Straub (Elsevier, Amsterdam, 1984), pp. 45–48.

[116] A. Stone, *The Theory of Intermolecular Forces*, International Series of Monographs on Chemistry (Clarendon, 1997).